Article

Energy-level matching of Fe(III) ions grafted at surface and doped in bulk for efficient visible-light photocatalysts

Min Liu, Xiaoqing Qiu, Masahiro Miyauchi, and Kazuhito Hashimoto

Just Accepted

Energy-level matching of Fe(III) ions grafted at surface and

doped in bulk for efficient visible-light photocatalysts

Min Liu,[‡] Xiaoqing Qiu,[‡] Masahiro Miyauchi,*[†,□] and Kazuhito Hashimoto*[‡,§]

[†]Department of Metallurgy and Ceramics Science, Graduate School of Science and Engineering, Tokyo Institute of Technology, 2-12-1 Ookayama, Meguro-ku, Tokyo 152-8552, Japan.

[‡]Research Center for Advanced Science and Technology, The University of Tokyo, 4-6-1 Komaba, Meguro-ku, Tokyo 153-8904, Japan.

[§]Graduate School of Engineering, The University of Tokyo, 7-3-1 Hongo, Bunkyo-ku, Tokyo 113-8656, Japan.

[□]Japan Science and Technology Agency (JST), PRESTO, 4-1-8 Honcho Kawaguchi, Saitama 332-0012, Japan.

Email: mmiyauchi@ceram.titech.ac.jp, hashimoto@light.t.u-tokyo.ac.jp

Abstract

Photocatalytic reaction rate (R) is determined by the multiplication of light absorption capability (α) and quantum efficiency (QE); however, these two parameters generally have trade-off relations. Thus, increasing α without decreasing QE remains a challenging issue for developing efficient photocatalysts with high R. Herein, using Fe(III) ions grafted Fe(III) doped TiO$_2$ as a model system, we present a novel method for developing visible-light photocatalysts with efficient R, utilizing the concept of energy level matching between surface-grafted Fe(III) ions as co-catalysts and bulk-doped Fe(III) ions as visible light absorbers. Photogenerated electrons in the doped Fe(III) states under visible light efficiently transfer to the surface grafted Fe(III) ions co-catalysts, as the doped Fe(III) ions in bulk produced energy levels below the conduction band of TiO$_2$, which match well with the potential of Fe^{3+}/Fe^{2+} redox couple in the surface grafted Fe(III) ions. Electrons in the surface

1

grafted Fe(III) ions efficiently cause multi-electron reduction of adsorbed oxygen molecules to achieve high *QE* value. Consequently, the present Fe(III)-Fe$_x$Ti$_{1-x}$O$_2$ nanocomposites exhibited the highest visible light *R* among the previously reported photocatalysts for decomposition of gaseous organic compounds. The high *R* can proceed even under commercial white light emission diode (LED) irradiation and is very stable for long-term use, making it practically useful. Further, this efficient method could be applied in other wide-band-gap semiconductors, including ZnO or SrTiO$_3$, and may be potentially applicable for other photocatalysis systems, such as water splitting and, CO$_2$ reduction, NO$_x$ removal, and dye decomposition. Thus, this method represents a strategic approach to develop new visible-light-active photocatalysts for practical uses.

1. Introduction

Heterogeneous photocatalysis using semiconductors has great potential for solving current energy and environmental issues.[1-20] Efficient photocatalysts are typically wide-band-gap semiconductors, such as TiO$_2$, ZnO, and SrTiO$_3$, owing to the high redox potential of photogenerated charge carriers.[10] Holes with high oxidation power in the valence band (VB) and electrons with sufficient reduction power in the conduction band (CB) are generally required for efficient photocatalytic reactions. However, wide-band-gap semiconductors are only activated under ultraviolet (UV) light irradiation, which limits their practical applications.

The doping of various transition metal cations or anions into wide-band-gap semiconductors has been extensively studied to increase the visible light absorption of these photocatalysts.[1-10] However, despite extensive research efforts, most systems remain unsatisfactory for practical use. In particular, metal-ion dopants introduce deep impurity levels in the forbidden band of semiconductor photocatalysts, where they act as recombination centers and impair photocatalytic activity.[1-4] In the case of anion-doped semiconductors, isolated states are formed above the VB and cause the quantum efficiency (*QE*) of the semiconductors to deteriorate, as the holes generated in these isolated states have

2

lower oxidation power and mobility than those in the VB.[1,2,6-9] For example, the QE of nitrogen-doped TiO_2 under visible light is markedly lower than that of pure TiO_2 under UV light.[6,9] These previous studies indicate that it is difficult to improve the visible-light absorption of semiconductors while maintaining a high QE value, because the reactivities of photogenerated charge carriers in doped levels or narrowed bands are much less than those in the VB and CB.

Very recently, our group demonstrated that the surface modification of TiO_2 with co-catalysts such as Cu(II) and Fe(III) ions[21-30] induces the efficient interfacial charge transfer[31-35] of VB electrons upon visible-light irradiation and multi-electron reduction reactions of oxygen,[36-44] during which the excited electrons are consumed. Co-catalysts also improve the visible-light activities of doped semiconductors.[25-30] For example, Ti^{3+} self-doped TiO_2, which is inactive even under UV light, functioned as an efficient visible-light photocatalyst upon the surface grafting of Cu(II) or Fe(III) co-catalysts.[28] These results indicate that a charge transfer occurs between photogenerated electrons from doped levels to the surface Cu(II) or Fe(III) co-catalysts. However, the reported QEs of these doped TiO_2 photocatalysts were markedly lower than that of Cu(II)- or Fe(III)-grafted undoped TiO_2, as the charge transfer is limited from doped levels to surface co-catalysts. But, the visible-light absorption capacity of Cu(II)- or Fe(III)-grafted undoped TiO_2 is relatively weak, as interfacial charge transfer occurs only at interfaces. Thus, such systems still exhibits low photocatalytic activities, which implies that it is difficult to improve QE in systems with high visible-light absorption. As a trade-off relation exists between visible-light absorption and QE, it is difficult to obtain large reaction rates (Rs) under visible-light irradiation for wide-band-gap semiconductors.

Herein, we developed an efficient visible-light photocatalyst based on matching the energy levels of surface-grafted and bulk-doped ions with similar energy states. We found that doping Fe(III) ions in bulk introduces energy levels in the band gap of TiO_2 that are similar to the redox potential of surface Fe(III) ions. The bulk-doped Fe(III) ions increase the visible-light absorption of TiO_2, while the surface-grafted Fe(III) ions help maintain the high QE of this photocatalyst. Thus, efficient visible-light photocatalysts with high Rs were obtained using

3

this approach. A high R was even achieved under white light emitting diode (LED) irradiation, and R values comparable to those of the best commercial TiO_2 photocatalysts, such as P-25 (Degussa), were obtained under UV light irradiation.

2. Experimental Section

2.1 Synthesis of $Fe_xTi_{1-x}O_2$ Samples. The Fe(III)-doped TiO_2 ($Fe_xTi_{1-x}O_2$) nanocomposites were prepared using a simple impregnation technique with commercial TiO_2 (rutile phase, 15-nm grain size, 90 m^2/g specific surface area; MT-150A, Tayca Co.) as the starting material. Briefly, 1.5 g TiO_2 powder was dispersed in 10 mL ethanol to form a TiO_2 suspension. $FeCl_3 \cdot 6H_2O$ (Wako, 99.9%), acting as the source of Fe(III), was weighed to give a weight fraction of Fe relative to TiO_2 of 0.1% and was added to the TiO_2 suspension, which was then stirred for 0.5 h in a vial reactor. The suspension was dried under a room temperature and the obtained residue was further heated at 950 °C for 3 h to form $Fe_xTi_{1-x}O_2$. The calcined $Fe_xTi_{1-x}O_2$ was treated with a 6 M HCl aqueous solution at 90 °C for 3 h under stirring. The products were filtered twice through a membrane filter (0.025 μm, Millipore) and then washed with sufficient amounts of distilled water. $Fe_xTi_{1-x}O_2$ was obtained as a clear powder and dried at 110 °C for 24 h. Subsequently, the obtained $Fe_xTi_{1-x}O_2$ was ground into a fine powder using an agate mortar and pestle for the preparation of Fe(III)-$Fe_xTi_{1-x}O_2$ nanocomposites. Pure TiO_2 was obtained using the same annealing and acid treatment process without adding $FeCl_3$ solution, and was used to prepare Fe(III)-TiO_2 nanocomposites.

2.2 Modification of $Fe_xTi_{1-x}O_2$ Samples with Fe(III) Ions. The grafting of Fe(III) ions onto $Fe_xTi_{1-x}O_2$ was performed using an impregnation method, as reported previously.[23] Briefly, 1 g $Fe_xTi_{1-x}O_2$ powder was first dispersed in 10 mL distilled water. $FeCl_3 \cdot 6H_2O$ (Wako, 99.9%) was weighed to give a weight fraction of Fe relative to $Fe_xTi_{1-x}O_2$ of 0.1% and was then added to the aqueous $Fe_xTi_{1-x}O_2$ suspension. The suspension was heated at 90 °C, stirred for 1 h in a vial reactor, and then filtered twice with a membrane filter (0.025 μm, Millipore) and washed with sufficient amounts of distilled water. The resulting residue was dried at 110 °C for 24 h and subsequently ground into fine powder using an agate mortar and pestle. Fe(III)-TiO_2 was also prepared by the same impregnation method.

4

2.3 Sample Characterizations. The structural characteristics of the prepared samples were measured by powder X-ray diffraction (XRD) at room temperature on a Rigaku D/MAX25000 diffractometer with a copper target (λ=1.54056 Å). Electron spin resonance (ESR) spectra were recorded on a Bruker ESP350E spectrometer. Elemental analyses of the samples were performed using an inductively coupled plasma-atomic emission spectrometer (ICP-AES, P-4010, Hitachi). [57]Fe Mössbauer spectra were measured at room temperature in a transmission geometry using a [57]Co/Rh source. UV−visible absorption spectra were obtained by the diffuse reflection method using a spectrometer (UV-2550, Shimadzu). The morphologies of the prepared $Fe_xTi_{1-x}O_2$ nanocomposites were investigated by scanning electron microscopy (SEM) using a Hitachi SU-8000 apparatus and transition electron microscopy (TEM) on a Hitachi HF-2000 instrument using an acceleration voltage of 200 kV. Surface compositions were studied by X-ray photoelectron spectroscopy (XPS; model 5600, Perkin-Elmer). The binding energy data were calibrated with reference to the C 1s signal at 284.5 eV.

2.4 Evaluation of Photocatalytic Properties. The photocatalytic activities of photocatalysts were evaluated by the decomposition of gaseous 2-propanol (IPA) under visible light, UV light, and white LED illumination. An Xe lamp (LA-251Xe, Hayashi Tokei) equipped with L-42, B-47, and C-40C glass filters (Asahi Techno-Glass) or a D-36A glass filter (Asahi Techno-Glass) was used as a source of visible light (420−530 nm, 1 mW/cm^2) and UV light (320-400 nm, 1 mW/cm^2), respectively. A commercial white LED (LDA 7A, 7.2 W; Toshiba, Co. Ltd.) located 15 cm from the sample was used as an indoor light source (1 mW/cm^2, ~300 lux). The light intensity was measured using a light radiometer (USR-45D, Ushio Co.) and was then adjusted to 1 mW/cm^2. A 500-mL cylindrical glass vessel was used as the photocatalysis reactor. To perform the photocatalytic experiments, 300 mg photocatalyst powder was first evenly spread on the bottom of a circular glass dish (area of 5.5 cm^2) that was mounted in the middle of the vessel reactor. The vessel was sealed with a rubber O-ring and a quartz cover, evacuated, and filled with fresh synthetic air. To eliminate organic contaminants on the sample surface, the vessel was illuminated with a Xe lamp (LA-251Xe) until the CO_2 generation rate was less than 0.02 μmol/day. The vessel was then

5

evacuated and refilled with fresh synthetic air. The pressure inside the vessel was kept at ~1 atm. Next, 300 ppmv (~6 μmol) of gaseous IPA was injected into the vessel. Prior to light irradiation, the vessel was kept in the dark for 12 h to achieve the absorption/desorption equilibrium of IPA on the photocatalyst surfaces. The IPA concentration first decreased and then remained constant, demonstrating the absorption/desorption equilibrium of IPA had been reached. During the equilibration process, no acetone or CO_2 were detected under dark conditions, demonstrating that the IPA molecules were not decomposed by the photocatalysts under dark conditions. The vessel was then irradiated with light, and 1 mL gaseous samples were periodically extracted from the reaction vessel to measure the concentrations of IPA, acetone, and CO_2 using a gas chromatograph (model GC-8A, Shimadzu Co., Ltd.).

2.5 Density of states (DOS) calculation. The plane-wave-based density functional theory (PW-DFT) calculations were performed for TiO_2 and $Fe_xTi_{1-x}O_2$ using the *ab initio* total-energy and the Vienna Ab initio Simulation Package (VASP) molecular dynamics program.[45,46] The Perdew-Burke-Ernzerhof (PBE) functional[47,48] of generalized gradient approximation (GGA) level was employed together with the pseudopotentials, which reduce the number of PWs to lower the maximum kinetic energy of the PW.[49] A 48-atom $2 \times 2 \times 2$ super cell was used for the calculation, in which a Ti atom was replaced with a Fe atom at the center of the super cell. The crystal model is shown in Figure S1. The moderate rate of substitution of Ti sites at the center of the super cell (6.25%) helped to reduce distortion of the tetragonal lattice.[50] The core orbitals were replaced by ultrasoft pseudopotentials with a kinetic energy cutoff of 500 eV. The density of the Monkhorst-Pack k-point sampling was $5 \times 5 \times 3$. The rutile phase of TiO_2 was used for the DOS calculation.

3. Results and Discussion

The DOSs of rutile TiO_2 and $Fe_xTi_{1-x}O_2$ were investigated using the plane-wave density functional theory program VASP. Figure 1a shows the DOS of pure TiO_2. The VB edge of TiO_2 consists mainly of O2p states, whereas the CB edge has predominantly Ti 3d character.[51] It should be noted that the calculated band gap is ~1.8 eV, which is markedly smaller than the experimental band gap of 3.0 eV due to well-known GGA error.[52] As illustrated in Figure 1b,

6

when Fe(III) ions were doped into TiO_2, the Fe 3d orbitals split into two bands.[53] The upper

band was hybridized with the CB and the interband was located 0.3- 0.5 eV below the CB of

TiO_2, a finding that is consistent with previous theoretical calculation results for Fe doped

TiO_2.[53] Considering the narrowing of the calculated value, the energy states of these interband

levels are close to the redox potential of Fe^{3+}/Fe^{2+} (E^0=0.771 V, vs SHE, pH=0)[54] in

surface-grafted Fe(III) ions, demonstrating that surface-grafted and bulk-doped Fe(III) have

nearly identical energy levels.

$Fe_xTi_{1-x}O_2$ photocatalysts were prepared from commercial rutile TiO_2 and $FeCl_3 \cdot 6H_2O$ using

a simple impregnation method and heat treatment. The grafting of Fe(III) ions onto $Fe_xTi_{1-x}O_2$

was performed by a similar impregnation method in a vial reactor.[23] Using ICP-AES, the total

amount of Fe in the obtained samples was found to be nearly equal to the initial value used in

the preparation process (Table S1). Upon surface grafting and bulk doping of Fe(III), the color

of the obtained powders changed from white to yellow (Figure S2), indicating that the

prepared photocatalyst was visible-light sensitive. Diffuse reflectance spectroscopy

measurements clearly showed that surface-grafted Fe(III) and bulk-doped Fe(III) similarily

increased visible-light absorption from 400 to 600 nm (Figure 2a). The difference absorption

spectra of Fe(III)-TiO_2, $Fe_xTi_{1-x}O_2$, and Fe(III)-$Fe_xTi_{1-x}O_2$ versus bare TiO_2 indicated that the

light absorption of Fe(III)-$Fe_xTi_{1-x}O_2$ was mainly attributed to the bulk-doped Fe(III) (Figure

2b). More importantly, the visible-light absorption peaks for $Fe_xTi_{1-x}O_2$ and Fe(III)-TiO_2 both

appeared around 420 nm. Taken together, these results indicate that the energy states of the

surface-grafted and bulk-doped Fe(III) ions have similar energy potential.

XRD patterns revealed that the prepared samples maintained a rutile TiO_2 crystalline

structure (JCPDS card No. 21-1276) after Fe(III) doping or surface Fe(III) grafting (Figure 3

and Figure S3), indicating that neither surface-grafted nor bulk-doped Fe(III) ions affect the

crystal phase of TiO_2. The sharp XRD peaks indicate that the products were highly

crystallized with approximate particle sizes of 130 nm according to Scherrer's equation[55].

ESR analysis revealed $Fe_xTi_{1-x}O_2$ had strong Fe(III) signals (Figure S4a), and the calculated

density of Fe(III) ions was 1.1×10^{19} per gram (/g), consistent with the amount of starting

Fe(III) source material (0.1 wt%). When Fe(III) ions were doped into TiO_2, a very weak Ti^{3+}

7

signal was observed in the ESR spectrum (Figure S4b). These Ti^{3+} species originated in oxygen vacancies and maintain the charge balance in Fe(III)-doped TiO_2.[56] However, the carrier density of Ti^{3+} species was only 6.8×10^{14} (/g), which was several orders of magnitude lower than that of Fe(III) (1.1×10^{19} (/g)). Therefore, the visible-light absorption by $Fe_xTi_{1-x}O_2$ is mainly due to the unoccupied Fe(III) species formed below the CB of TiO_2.

SEM images (Figure S5) revealed that all of the prepared Fe(III)-$Fe_xTi_{1-x}O_2$ photocatalysts were assemblies of uniformly distributed nanoparticles. Introduction of Fe(III) ions on the TiO_2 surface as well as into the TiO_2 lattice did not change the morphology or particle size of the obtained Fe(III)-$Fe_xTi_{1-x}O_2$ samples. The average grain size of the nanoparticles was approximately 200 nm, which is close to the estimated crystallite size, confirming that the samples were highly crystallized.

XPS spectra were recorded to determine the surface composition and chemical states of the surface elements (Figure 4 and Figure S6). In the Ti 2p core-level spectra of the samples (Figure 4a), no obvious differences could be seen in the chemical states of element Ti,[57] demonstrating that neither the surface grafting nor bulk doping of Fe(III) ions affected the bonding structure between titanium and oxygen. In the Fe 2p core-level spectra (Figure 4b), Fe signals were only observed in Fe(III)-grafted samples, such as Fe(III)-TiO_2 and Fe(III)-$Fe_xTi_{1-x}O_2$, confirming that Fe(III) was successfully grafted on the surface of TiO_2 and $Fe_xTi_{1-x}O_2$. Fe signals were also detected in wide-scanned XPS spectra (Figure S6) of Fe(III)-TiO_2 and Fe(III)-$Fe_xTi_{1-x}O_2$. According to our previous X-ray absorption fine structure (XAFS) measurements and XPS analysis of the Fe(III)-TiO_2 system,[23] these signals can be assigned to iron ions with an oxidation number of three. Based on these analyses of local crystal structure, Fe(III) ions were grafted as distorted amorphous FeOOH-like structures. In addition, the chemical state and environment of surface Fe(III) ions in the present Fe(III)-TiO_2 and Fe(III)-$Fe_xTi_{1-x}O_2$ samples are similar to those of the previous Fe(III)-TiO_2 system. Notably, no Fe(III) signal was detected for $Fe_xTi_{1-x}O_2$, as Fe(III) ions were doped in bulk and the intensity of surface-doped ions was below the detection limit of the XPS analysis.

To explore the states of surface-grafted and bulk-doped Fe(III) in more detail, Mössbauer spectra and TEM images were recorded. The nuclear ground and excited levels involved in

the Mössbauer transition were shifted or split because of the electrostatic interactions between the nuclear charge and the surrounding electric charge.[58] As shown in Figure 5a, clear signals were seen in $Fe(III)-TiO_2$, $Fe_xTi_{1-x}O_2$, and $Fe(III)-Fe_xTi_{1-x}O_2$, whereas no signal was observed for pure TiO_2. Both $Fe_xTi_{1-x}O_2$ and $Fe(III)-TiO_2$ exhibited quadrupole splitting and had isomer shifts of around 0.38 mm/sec, indicating that both the bulk-doped and surface-grafted Fe(III) ions are in paramagnetic states with a quadrupole doublet as an octahedral structure.[59-63] The spectral peaks of $Fe(III)-Fe_xTi_{1-x}O_2$ could be perfectly fitted by the simple addition of spectra for $Fe_xTi_{1-x}O_2$ and $Fe(III)-TiO_2$ in equal proportion. It is noteworthy that the quadrupole shifts for the surface-grafted and bulk-doped Fe(III) ions were different. The quadrupole split for Fe(III)-doped TiO_2 was 0.51 mm/sec, whereas that for Fe(III)-grafted TiO_2 was 0.77 mm/sec, indicating that surface Fe(III) ions have a larger structural degree of freedom as compared to doped Fe(III) ions.[59-63] Further, the ionic radius of Ti^{4+} with six coodination is 0.061 nm, which is as large as that of Fe^{3+} (0.064 nm).[2,3,53] These results indicate that doped Fe(III) ions are substitutionally introduced into TiO_2 crystal at Ti^{4+} sites,[59-63] whereas surface-grafted Fe(III) ions exist as amorphous nanoclusters, consistent with our previous study of $Fe(III)-TiO_2$.[23] TEM images (Figure 5b and Figure S7) confirmed that amorphous Fe(III) nanoclusters of ~2 nm in size were well dispersed on the surface of $Fe_xTi_{1-x}O_2$. In addition, we observed good attachment of Fe(III) nanoclusters on the $Fe_xTi_{1-x}O_2$ surfaces. The clear lattice fringes of the nanoparticles demonstrated that the $Fe_xTi_{1-x}O_2$ was highly crystallized.

The photocatalytic activities of the prepared photocatalysts were evaluated by the decomposition of gaseous IPA under visible-light irradiation. IPA was selected as a representative volatile organic compound (VOC) as it is reported to be a serious pollutant of indoor air.[64] The oxidation of IPA to CO_2 and its usefulness for the determination of *QE* have been comprehensively established.[64] The wavelength of the visible light source used in the analysis was 400-530 nm, and the light intensity was 1 mW/cm^2 (Figure S8), which corresponds to an illuminance of only 300 lux and is comparable to the intensity of white fluorescent lights and white LED lights. For the performance tests, the initial concentration of IPA was 300 ppmv (~6 μmol), which is much higher than the VOC concentrations typically encountered in indoor environments. Under these conditions, the complete decomposition of

9

IPA would result in a CO_2 concentration of 900 ppmv (~18 μmol), which is three times of IPA concentration. A representative time course of the gas concentrations during the decomposition of IPA by the Fe(III)-$Fe_xTi_{1-x}O_2$ sample is shown in Figure S9.

Figure 6a shows CO_2 evolution from IPA decomposition by Fe(III)-grafted TiO_2 doped with various metal ions. Among the examined metal dopants, Fe(III)-$Fe_xTi_{1-x}O_2$ nanocomposites exhibited the best performance, completely decomposing gaseous IPA to CO_2 within 30 h. The CO_2 generation rate achieved by Fe(III)-$Fe_xTi_{1-x}O_2$ was 0.69 μmol/h (Figure S10), which is the highest R among reported visible-light photocatalysts. The high visible-light activity of Fe(III)-$Fe_xTi_{1-x}O_2$ is due to the similar energy levels of surface Fe(III) and bulk Fe(III). Comparatively, $TiO_{2-x}N_x$, which is recognized as one of the most efficient visible-light photocatalysts,[6] exhibited rather low activity, 0.16 μmol CO_2/h, and required over 300 h to completely decompose the gaseous IPA (Figure S11). The low activity of this system is attributable to the markedly lower oxidation power of the photogenerated holes in the nitrogen levels than those in the VB.[9]

The importance of energy level matching between surface-grafted and bulk-doped Fe(III) ions was further demonstrated by comparative studies of the photocatalytic activities of bare $Fe_xTi_{1-x}O_2$, Fe(III)-TiO_2, and Fe(III)-$Fe_xTi_{1-x}O_2$ (Figure 6b). After doping Fe(III) ions in bulk, $Fe_xTi_{1-x}O_2$ became sensitive to visible light, but exhibited relatively low R and QE values (Table 1). Fe(III)-TiO_2 also exhibited significant visible-light activity, as the surface-grafted Fe(III) ions acted as a co-catalyst and effectively consumed the photogenerated electrons through efficient interfacial charge transfer and multi-electron reduction reactions,[31-44] resulting in a high QE (53.5%). However, the R of Fe(III)-TiO_2 remained low due to the limited visible-light absorption by this photocatalyst (Figure 2 and Table 1). In contrast, after the selected surface grafting and bulk doping of Fe(III) ions to achieve closely matched energy levels, the Fe(III)-$Fe_xTi_{1-x}O_2$ nanocomposites demonstrated strong visible-light absorption with a QE of 47.3% as a result of efficient light absorption by bulk-doped Fe(III) and electron transfer between the doped and surface-grafted Fe(III) ions, as well as efficient multi-electron reduction on the surface Fe(III) nanoclusters.[23,36-44] Due to these excellent properties, the Fe(III)-$Fe_xTi_{1-x}O_2$ nanocomposites exhibited a high R.

10

We next examined the visible-light activity of Fe(III)-$Fe_xTi_{1-x}O_2$ nanocomposites under conditions mimicking actual indoor environments. White LED, which is widely used as an indoor light source, does not emit UV light (Figure S12) can therefore be used to examine the true visible-light activity of photocatalysts. Under white LED irradiation with a light intensity of 1 mW/cm^2, the Fe(III)-$Fe_xTi_{1-x}O_2$ nanocomposites completely decomposed IPA to CO_2 (Figure S13). We also evaluated the photocatalytic activity of commercial P-25 TiO_2, which is considered to be an efficient UV-light photocatalyst,[10] under UV light irradiation with the same light intensity as white LED (1 mW/cm^2). The R of Fe(III)-$Fe_xTi_{1-x}O_2$ under white LED was 0.29 μmol/h, which is 16% of the R value of P-25 under UV-light irradiation (1.78 μmol/h). This visible-light activity of Fe(III)-$Fe_xTi_{1-x}O_2$ is markedly higher than those of previously reported visible-light photocatalysts, which were two orders of magnitude lower than that of pure TiO_2 under UV light.[9,65] Notably, the absorbed photon number of Fe(III)-$Fe_xTi_{1-x}O_2$ under white LED irradiation in the present experimental conditions was approximately 16% of that of P-25 under UV irradiation. However, the QE of Fe(III)-$Fe_xTi_{1-x}O_2$ under indoor light irradiation was as high as that of commercial P-25 under UV irradiation. Therefore, Fe(III)-$Fe_xTi_{1-x}O_2$ is expected to be usable for various indoor applications, as its photocatalytic performance under indoor light is comparable to that of P-25 under sunlight.

In addition to performance, the stability of photocatalysts is critical for practical applications. Previous studies have reported that doped elements are unstable under light irradiation, as they are often oxidized or reduced during excitation.[66-70] Thus, the photocatalytic activities of doped metal oxides tend to decrease under long-term light illumination. For example, Chen et al.[67] reported that the photocatalytic capability of N-doped TiO_2 decreases gradually due to the oxidation of lattice nitrogen by photogenerated holes during the degradation reaction, leading to photocatalytic instability. In our present system, photogenerated electrons are efficiently transferred to surface Fe(III) and consumed in efficient reduction reaction processes due to the good energy level matching of surface-grafted and bulk-doped Fe(III) ions. We demonstrated that the high performance of Fe(III)-$Fe_xTi_{1-x}O_2$ could be maintained under repeated light irradiation in air for 1 year, as

11

shown in Figure 6c, and estimated that the turnover number of this system exceeded 80. In addition, we optimized the various experimental conditions and found that 0.1 wt% was the optimal amount of both doped and surface-grafted Fe(III) ions (Figures S14 and S15). The Fe(III)-$Fe_xTi_{1-x}O_2$ sample was also very active under UV-light irradiation. Thus, the high photocatalytic activity and stability of Fe(III)-$Fe_xTi_{1-x}O_2$ indicates that this photocatalyst has great potential for practical applications.

To further investigate the influence of energy level matching of surface-grafted and bulk-doped Fe(III) ions, we changed the surface Fe(III) to Cu(II), which is also reported to be an efficient co-catalyst.[21,22] However, the activity of the prepared Cu(II)-$Fe_xTi_{1-x}O_2$ sample was clearly decreased under the same light irradiation conditions used for Fe(III)-$Fe_xTi_{1-x}O_2$ (Figure S16). As the reported redox potential of Cu^{2+}/Cu^+ is 0.16 V (vs. SHE, pH=0),[54] the energy level of surface Cu(II) is not matched with that of the bulk-doped Fe(III) ions. Further, we prepared photocatalysts with Cu(II) ions as dopants in place of Fe(III). However, the photocatalytic activities of Fe(III)-$Cu_xTi_{1-x}O_2$ and Cu(II)-$Cu_xTi_{1-x}O_2$ were very low, because the states of the doped Cu(II) ions appeared at much deeper levels in the band gap, locating at the upside of VB.[71] Particularly, the activity of Fe(III)-$Cu_xTi_{1-x}O_2$ is higher than that of Cu(II)-$Cu_xTi_{1-x}O_2$, further proved the deeper energy levels of doped Cu(II) ions, because the redox potential of Fe^{3+}/Fe^{2+}, 0.771 V, is more positive than that of Cu^{2+}/Cu^+, 0.16 V. Thus, the activity of Cu(II)-$Cu_xTi_{1-x}O_2$ was negligible (Figure S17), owing to the large energy level difference between the surface-grafted and bulk-doped Cu(II) ions.[54,71] Based on these results, the photocatalytic mechanisms operating in the Fe(III)-$Fe_xTi_{1-x}O_2$ system are proposed, as illustrated in Figure 7. Pure TiO_2 is inactive under visible light owing to its wide band gap. After the selected surface grafting and bulk doping of Fe(III) ions, which have closely matched energy levels, the visible-light absorption of TiO_2 was drastically enhanced by the bulk-doped Fe(III) ions and the *QE* was unaffected because of the efficient transfer of electrons between doped Fe(III) and surface Fe(III), which acts as an efficient co-catalyst for multi-electron reduction reactions. Moreover, a good junction between surface-grafted and bulk-doped Fe(III) ions was also critical for the efficient charge transfer. Notably, if a thin

12

layer was introduced between the surface Fe(III) ions and doped TiO_2 (Figure S18), the visible-light activity was markedly reduced (Figure S19).

In the present paper, using Fe(III) ions grafted Fe(III) doped TiO_2 as a model system, we comprehensively studied energy level matching between surface-grafted Fe(III) ions as co-catalysts and bulk-doped Fe(III) ions as visible light absorbers. It has been confirmed that our concept is applicable for not only TiO_2 as a metal oxide semiconductors, but also other semiconductor photocatalysts, including zinc oxide (ZnO) and strontium titanate ($SrTiO_3$), as described in the Supporting Information (Figure S20). Further, the energy level matching of surface-grafted and bulk-doped Fe(III) ions is just one example of a photocatalytic reaction involving oxygen reduction. Although Fe(III) ion nanoclusters are reported to be effective cocatalysts for oxygen reduction,[23] a number of other cocatalysts, including Cu(II), Pt, Rh, NiO_x, RuO_2, and IrO_2, have been have been reported to enhance the charge separation efficiencies for various photocatalytic reactions, including water splitting, CO_2 reduction, NO_x removal, and organic and dye decomposition.[21-24,27-30,71-76] For example, we have previously shown that the coupling of cerium (Ce) doping and copper (Cu) grafting on zinc oxide (ZnO) is also very effective for constructing visible-light-sensitive photocatalysts.[29] Since the energy level of doped Ce is similar to that of surface-grafted Cu(II) ions, Ce-doped ZnO grafted with Cu(II) ions exhibits visible-light activity. Our concept of matching the energy levels of dopants with the redox potential of surface-grafted ions may help researchers identify suitable systems for target photocatalytic reactions. We believe that our concept of energy matching between surface-grafted and bulk-doped metal ions is not limited to reaction systems of specific semiconductor materials, but represents a general strategy for developing new visible-light-sensitive photocatalysts.

4. Conclusions

We have developed a novel visible-light-driven photocatalyst based on the concept of energy level matching between surface-grafted and bulk-doped Fe(III) ions. Our findings show that bulk-doped Fe(III) ions produce energy levels below the CB of TiO_2, which match well with the redox potential of the surface-grafted Fe(III) ions. The doping of Fe(III) ions

13

increase the visible-light absorption of TiO_2, while the surface grafting of Fe(III) ions maintains the high *QE* of this oxide. Due to the close energy level matching of bulk and surface Fe(III), electrons on the former were transferred to the latter, thereby efficiently driving oxygen reduction. Thus, the present Fe(III)-$Fe_xTi_{1-x}O_2$ nanocomposites exhibited strong visible-light absorption and maintained a high *QE*, leading to the highest visible light *R* among reported photocatalysts for the decomposition of gaseous organic compounds. A high *R* was achieved even under commercial white LED irradiation and was stable during long-term use, demonstrating the practical utility of this photocatalyst. Further, the developed nanocomposites are composed of ubiquitous and safe elements. Notably, the energy level matching method described here can potentially be applied to other wide-band-gap semiconductors and photocatalysis systems. Thus, our present findings open a new avenue for constructing advanced visible-light photocatalysts for practical use.

Supporting Information Available: Table S1, the amount of Fe(III) in the sample derived from ICP-AES spectrophotometry. Figure S1, Crystal models. Figures S2, photos of samples. Figure S3, XRD patterns of $Fe_xTi_{1-x}O_2$. Figure S4, ESR spectra of Fe(III)-$Fe_xTi_{1-x}O_2$. Figure S5, SEM images of samples. Figure S6, full-scale XPS spectra of samples. Figures S7, TEM images of samples. Figure S8, light source for the visible-light irradiation. Figure S9, time course of gas concentrations during the decomposition of IPA by Fe(III)-$Fe_xTi_{1-x}O_2$. Figure

14

S10, details of the quantum efficiency calculations. Figure S11, photocatalytic activities of TiO_2, $TiO_{2-x}N_x$, and Fe(III)-$Fe_xTi_{1-x}O_2$. Figure S12, UV and LED indoor light source. Figure S13, comparative studies of CO_2 generation over Fe(III)-$Fe_xTi_{1-x}O_2$ under white LED irradiation and P-25 under UV light irradiation with the same light intensity. Figures S14 and S15 comparative evaluation of CO_2 generation by Fe(III)-grafted and bulk-doped samples under visible-light irradiation. Figure S16, comparative studies of CO_2 generation by Fe(III)-$Fe_xTi_{1-x}O_2$, Cu(II)-$Fe_xTi_{1-x}O_2$, and Fe(III)-$Cu_xTi_{1-x}O_2$. Figures S17, CO_2 generation by Fe(III)-$Fe_xTi_{1-x}O_2$ and Cu(II)-$Cu_xTi_{1-x}O_2$. Figure S18 and S19, Fe(III)-$Fe_xTi_{1-x}O_2$ with a thin layer between the surface-grafted and and bulk-doped Fe(III) ions. Figure S20, UV-Vis spectra and comparative studies of CO_2 generation by other semiconductors. This material is available free of charge via the internet at http://pubs.acs.org.

References

(1)   Thompson, T. L.; Yates, J. T.; *Chem. Rev.* **2006**, *106*, 4428-4453.

(2)   Chen, X.; Mao, S. S. *Chem. Rev.* **2007**, *107*, 2891-2959.

(3)   Hoffmann, S. T. Martin, W. Y. Choi, D. W. Bahnemann, *Chem. Rev.* **1995**, *95*, 69-96.

(4)   Highfield, J. G.; Pichat, P. *New. J. Chem.* **1989**, *13*, 61–66.

(5)   Chen, X.; Liu, L.; Yu, P. Y.; Mao, S. S. *Science* **2011**, *331*, 746-750.

(6)   Asahi, R.; Morikawa, T.; Ohwaki, T.; Aoki, K.; Taga, Y. *Science* **2001**, *293*, 269-271.

(7)   Khan, S. U. M.; Al-Shahry, M.; Ingler Jr., W. B. *Science* **2002**, *297*, 2243-2245.

(8)   Choi, W. Y.; Termin, A.; Hoffmann, M. R. *J. Phys. Chem.* **1994**, *98*, 13669-13679.

(9)   Irie, H.; Watanabe, Y.; Hashimoto, K. *J. Phys. Chem. B* **2003**, *107*, 5483-5486.

(10)   Ohtani, B.; *Chem. Lett.* **2008**, *37*, 216-229.

(11)   Liu, M.; Piao, L. Y.; Zhao, L.; Ju, S. T.; Yan, Z. J.; He, T.; Zhou, C. L.; Wang, W. J. *Chem. Commun.* **2010**, *46*, 1664-1666.

(12)   Liu, M.; Piao, L. Y.; Lu, W. M.; Ju, S. T.; Zhao, L.; Zhou, C. L.; Li, H. L.; Wang, W. J. *Nanoscale* **2010**, *2*, 1115-1117.

15

(13)   Li, H. M.; Zeng, Y. S.; Huang, T. C.; Piao, L. Y.; Yan, Z. J.; Liu, M. *Chem. Eur. J.* **2012**, *18*, 7525-7532.

(14)   Li, H. M.; Zeng, Y. S.; Huang, T. C.; Piao, L. Y.; Liu, M. *ChemPlusChem* **2012**, *77*, 1017-1021.

(15)   Kisch, H.; Zhang, L.; Lange, C.; Maier, W. F.; Antonius, C.; Meissner, D. *Angew. Chem. Int. Ed.* **1998,** *37*, 3034-3036.

(16)   Abe, R.; Takami, H.; Murakami, N.; Ohtani, B. *J. Am. Chem. Soc.* **2008**, *130*, 7780-7781.

(17)   Tada, H.; Jin, Q.; Nishijima, H.; Yamamoto, H.; Fujishima, M.; Okuoka, S.; Hattori, T.; Sumida, Y.; Kobayashi, H. *Angew. Chem. Int. Ed.* **2011**, *50*, 3501-3505.

(18)   Liu, M.; Piao, L. Y.; Wang, W. J. *J. Nanosci. Nanotech.* **2010**, *10*, 7469-7472.

(19)   Liu, M.; Piao, L. Y.; Ju, S. T.; Lu, W. M.; Zhao, L.; Zhou, C. L.; Wang, W. J. *Mater. Lett.* **2010**, *64*, 1204-1207.

(20)   Wu, Q.; Liu, M.; Wu, Z. J.; Li, Y. L.; Piao, L. Y. *J. Phys. Chem. C.* **2012**, *116*, 26800-26804.

(21)   Irie, H.; Miura, S.; Kamiya, K.; Hashimoto, K. *Chem. Phys. Lett.* **2008**, *457*, 202-205.

(22)   Irie, H.; Kamiya, K.; Shibanuma, T.; Miura, S.; Tryk, D. A.; Yokoyama, T.; Hashimoto, K. *J. Phys. Chem. C* **2009**, *113*, 10761-10766.

(23)   Yu, H. G.; Irie, H.; Shimodaira, Y.; Hosogi, Y.; Kuroda, Y.; Miyauchi, M.; Hashimoto, K. *J. Phys. Chem. C* **2010**, *114*, 16481-16487.

(24)   Qiu, X. Q.; Miyauchi, M.; Sunada, K.; Minoshima, M.; Liu, M.; Lu, Y.; Li, D.; Shimodaira, Y.; Hosogi, Y.; Kuroda, Y.; Hashimoto, K. *ACS Nano* **2012**, *6*, 1609-1618.

(25)   Yu, H. G.; Irie, H.; Hashimoto, K. *J. Am. Chem. Soc.* **2010***, 132*, 6898-6899.

(26)   Qiu, X. Q.; Miyauchi, M.; Yu, H. G.; Irie, H.; Hashimoto, K. *J. Am. Chem. Soc.* **2010***, 132*, 15259-15267.

(27)   Anandan, S.; Ohashi, N.; Miyauchi, M. *Appl. Catal. B* **2010**, *100*, 502-509.

(28)   Liu, M.; Qiu, X. Q.; Miyauchi, M.; Hashimoto, K. *Chem. Mater.* 2011, *23*, 5282−5286.

(29)   Anandan, S.; Miyauchi, M. *Phys. Chem. Chem. Phys.* **2011**, *13*, 14937-14945.

(30)   Anandan, S.; Miyauchi, M. *Electrochem.* **2011**, *79*, 842-844.

16

(31) Creutz, C.; Brunschwig, B. S.; Suntin, N. *J. Phys. Chem. B* **2005**, *109*, 10251-10260.

(32) Creutz, C.; Brunschwig, B. S.; Suntin, N. *J. Phys.Chem. B* **2006**, *110*, 25181-25190.

(33) Hush, N. S. *Electrochim. Acta* **1968**, *13*, 1005-1023.

(34) Hush, N. S. *J. Electroanal. Chem.* **1999**, *460*,5-29.

(35) Hush, N. S. *J. Electroanal. Chem.* **1999**, *470*, 170-195.

(36) Himo, F.; Eriksson, L. A.; Maseras, F.; Siegbahn, P. E. M. *J. Am. Chem. Soc.* **2000**, *122*, 8031-8036.

(37) Goldstein, S.; Czapski, G.; Eldik, R.; Cohen, H.; Meyerstein, D. *J. Phys. Chem.* **1991**, *95*, 1282-1285.

(38) Kitajima, N.; Morooka, Y. *Chem. Rev.* **1994**, *94*, 737-757.

(39) Cole, A.P.; Root, D. E.; Mukherjee, P.; Solomon, E. I.; Stack, T. D. P. *Science* **1996**, *273*, 1848-1850.

(40) Abe, R.; Takami, H.; Murakami, N.; Ohtani, B. *J. Am. Chem. Soc.***2008**, *130*, 7780-7781.

(41) Zhao, Z. G.; Miyauchi, M. *Angew. Chem., Int. Ed.* **2008**, *47*, 7051-7055.

(42) Arai, T.; Horiguchi, M.; Yanagida, M.; Gunji, T.; Sugihara, H.; Sayama, K. *Chem. Commun.* **2008**, 5565-5567.

(43) Kim,Y. H.; Irie, H.; Hashimoto, K. *Appl. Phys. Lett.* **2008**, *92*, 182107.

(44) Arai, T.; Yanagida, M.; Konishi, Y.; Iwasaki, Y.; Sugihara, H.; Sayama, K. *Catal. Commun.* **2008**, *9*, 1254-1258.

(45) Kresse, G.; Hafner, J. *Phys. Rev. B* **1993**, *48*, 13115-13118.

(46) Kresse, G.; Furthmuller, J. *Phys. Rev. B* **1996**, *54*, 11169-11186.

(47) Perdew, J. P.; Burke, K.; and Ernzerhof, M. *Phys. Rev. Lett.* **1996**, *77*, 3865-3868.

(48) Perdew, J. P.; Burke, K.; and Ernzerhof, M. *Phys. Rev. Lett.* **1997**, *78*, 1396-1396.

(49) Vanderbilt, D. *Phys. Rev. B* **1990**, *41*, 7892-7895.

(50) Yu, X. H.; Li, C. S.; Ling, Y.; Tang, T. A.; Wu, Q.; Kong, J. J.; *J. Alloy. Compd.* **2010**, *507*, 33-37.

(51) Henderson, M. A. A. *Surf. Sci. Rep.* **2011**, *66*, 185-297.

(52) Gai, Y. Q.; Li, J. B.; Li, S. S.; Xia, J. B.; and Wei, S. H.; *Phys. Rev. Lett.* **2009**, *102*, 036402.

(53) Wen, L. P.; Liu, B. S.; Zhao, X. J.; Nakata, K.; Murakami, T.; and Fujishima, A. *Int. J. Photoenergy* **2012**, *2012*, 368750.

(54) Bard, A.J.; Parsons, R.; Jordan, J. *Standard Potentials in Aqueous Solution,* Marcel Dekker, New York, **1985**.

(55) Cullity, B.D.; Stock, S.R. *Elements of X-Ray Diffraction*, 3rd Ed., Prentice-Hall Inc., New Jersey, **2001**.

(56) Bapna, K.; Choudhary, R. J.; Pandey, S. K.; Phase, D. M.; Sharma, S. K.; Knobel, M. *Appl. Phys. Lett.* **2011**, *99*, 112502.

(57) Oku, M.; Wagatsuma, K.; Kohiki, S. *Phys. Chem. Chem. Phys.* **1999**, *1*, 5327-5331.

(58) Millet, J. M. *Adv. Catal.* **2007**, *51*, 309–350.

(59) Pan, X.; Jiang, D.; Lin, Y.; Ma, X. *J. Magn. Magn. Mater.* **2006**, *305*, 388-391.

(60) Lee, H. M.; Kim, C. S. *J. Magn. Magn. Mater.* **2007**, *310*, 2099-2101

(61) Balcells, L.; Frontera, C.; Sandiumenge, F.; Roig, A.; Martinez, B.; Kouam, J.; Monty, C. *Appl. Phys. Lett.* **2006**, *89*, 122501.

(62) Lin, F.; Jiang, D. M.; Lin, Y.; Ma, X. M.; *Physica B* **2008**, *403*, 2193-2196.

(63) Cabrera, A. F.; Rodriguez Torres, C. E.; Errico, L.; Sanchez, F. H. *Physica B* **2006**, *384*, 345-347.

(64) Ohko, Y.; Hashimoto, K.; Fujishima, A. *J. Phys. Chem. A* **1997**, *101*, 8057-8062.

(65) Miyauchi, M.; Ikezawa, A.; Tobimatsu, H.; Irie, H.; Hashimoto, K. *Phys. Chem. Chem. Phys.* **2004**, *6*, 865-870.

(66) Koudriachova, M. V.; Harrison, N. M. *J. Mater. Chem.* **2006**, *16*, 1973-1977.

(67) Chen, X. F.; Wang, X. C.; Hou, Y. D.; Huang, J. H.; Wu, L.; Fu, X. Z. *J. Catal.* **2008**, *255*, 59-67.

(68) Mowbray, D. J.; Martinez, J. I.; Garcia Lastra, J. M.; Thygesen, K. S.; Jacobsen, K. W. *J. Phys. Chem. C* **2009**, *113*, 12301-12308.

(69) Braconnier, B.; Paez, C. A.; Lambert, S.; Alie, C.; Henrist, C.; Poelman, D.; Pirard, J. P.; Cloots, R.; Heinrichs, B. *Microporous Mesoporous Mater.* **2009**, **122**, 247-254.

18

(70)   Hanaor, D. A. H.; Assadi, M. H. N.; Li, S.; Yu, A. B.; Sorrell, C. C. *Comput. Mech.* **2012**, *50*,185–194.

(71)   Errico, L. A.; Rentería, M.; Weissmann, M. *Phys. Rev. B* **2005**, *72*, 184425.

(72)   Moon, S. C.; Mametsuka, H.; Suzuki, S.; and Anpo, M.; *Chem. Lett.* **1998**, *27*, 117-118.

(73)   Yamaguti, K.; Sato, S.; *J. Chem. Soc., Faraday Trans. 1* **1985**, *81*, 1237-1246.

(74)   Shimizu, K.; Itoh, S.; Hatamachi, T,; Kodama, T., Sato, M.; Toda, K.; *Chem. Mater.* **2005**, *17*, 5161-5166.

(75)   Yuan, Y.; Zheng, J.; Zhang, X.; Li, Z.; Yu, T.; Ye. J.; Zou, Z.; *Solid Sate Ionics* **2008**, *178,* 1711-1713.

(76)   Abe, R.; Higashi, M.; Domen, K.; *J. Am. Chem. Soc.* **2010**, *132*, 11828-11829.

19

Table 1. Performances of the indicated photocatalysts.

Sample	$TiO_{2-x}N_x$	$Fe_xTi_{1-x}O_2$	$Fe(III)-TiO_2$	$Fe(III)-Fe_xTi_{1-x}O_2$
R^i_p *(quanta/sec)*	1.30×10^{16}	1.30×10^{16}	1.30×10^{16}	1.30×10^{16}
R^a_p *(quanta/sec)*	4.10×10^{15}	1.39×10^{15}	7.48×10^{14}	1.46×10^{15}
R_{co2} *(µmol/h)*	0.16	0.09	0.40	0.69
QE *(%)*	3.9	6.5	53.5	47.3

R^i_p, rate of incident photons.

R^a_p, absorbed photon number.

R_{co2}, CO_2 generation rate.

20

Figure captions.

Figure 1. DOSs for (a) rutile TiO_2 and (b) $Fe_xTi_{1-x}O_2$ (x=0.0625). The tops of the VBs are assigned as 0 eV.

Figure 2. (a) UV-visible reflectance spectra of TiO_2, Fe(III)-TiO_2 $Fe_xTi_{1-x}O_2$ and Fe(III)-$Fe_xTi_{1-x}O_2$ nanocomposites. (b) Difference UV-vis spectra versus bare TiO_2 for Fe(III)-TiO_2, $Fe_xTi_{1-x}O_2$ and Fe(III)-$Fe_xTi_{1-x}O_2$ nanocomposites at x=0.1 wt%.

Figure 3. XRD patterns of bare TiO_2, Fe(III)-TiO_2, $Fe_xTi_{1-x}O_2$, and Fe(III)-$Fe_xTi_{1-x}O_2$ nanocomposites at x=0.1 wt%.

Figure 4. (a) Ti 2p core-level spectra and (b) Fe 2p core-level spectra of bare TiO_2, Fe(III)-TiO_2, $Fe_xTi_{1-x}O_2$, and Fe(III)-$Fe_xTi_{1-x}O_2$ nanocomposites at x=0.1 wt%.

Figure 5. (a) Mössbauer spectra of bare TiO_2, Fe(III)-TiO_2, $Fe_xTi_{1-x}O_2$, and Fe(III)-$Fe_xTi_{1-x}O_2$ nanocomposites at x=0.1 wt%. (b) HRTEM images of Fe(III)-$Fe_xTi_{1-x}O_2$. Fe(III) nanoclusters are indicated by the dotted lines. The good attachment of Fe(III) nanoclusters to $Fe_xTi_{1-x}O_2$ nanoparticles can be clearly observed.

Figure 6. (a) CO_2 generation curves for Fe(III)-$M_xTi_{1-x}O_2$ (M=Fe, Ce, Cu, and Ni, x=0.1 wt%) samples under visible-light irradiation. (b) Comparative studies of CO_2 generation by bare $Fe_xTi_{1-x}O_2$, Fe(III)-TiO_2, and Fe(III)-$Fe_xTi_{1-x}O_2$ at x=0.1 wt%, respectively. (c) Cycling measurements of the IPA decomposition over Fe(III)-$Fe_xTi_{1-x}O_2$ at x=0.1 wt% under visible-light irradiation. Experiments were conducted over a 12-month period.

Figure 7. Proposed photocatalysis processes. Pure TiO_2 is inactive for the visible light owing to its wide band gap. After selected surface grafting and bulk doping of Fe(III) ions, which have closely matched energy levels, the visible-light absorption of TiO_2 is drastically enhanced by the bulk-doped Fe(III) ions and the photogenerated electrons can be effectively transferred to the surface Fe(III), which acts as an efficient co-catalyst for multi-electron reduction reactions. Holes with high oxidation power are kept in the deep level of VB and decompose the organic compounds efficiently. Thus, efficient visible light photocatalysts with high R are achieved.
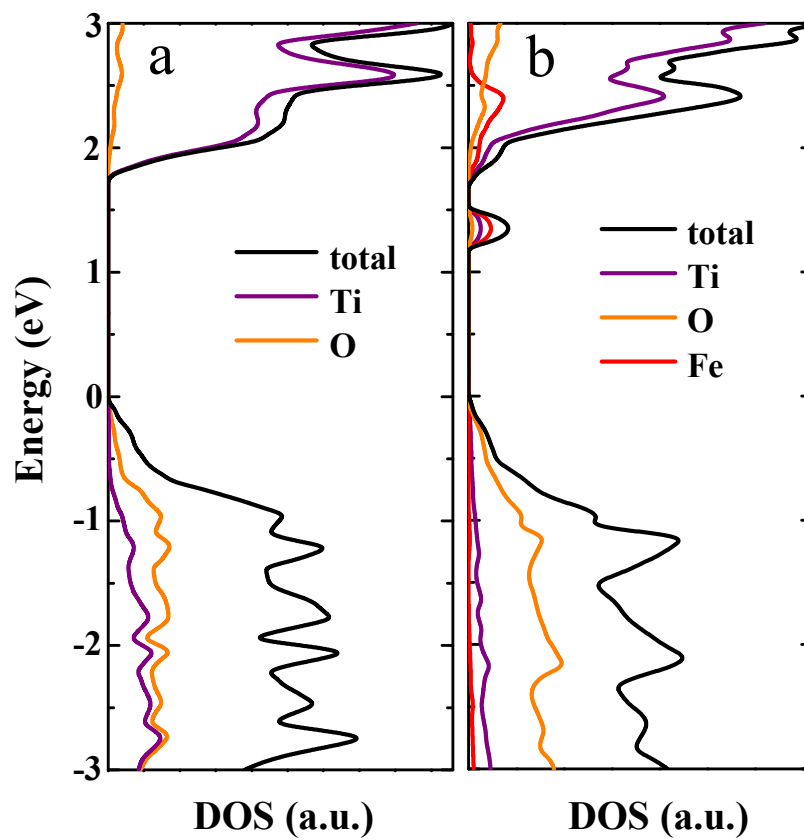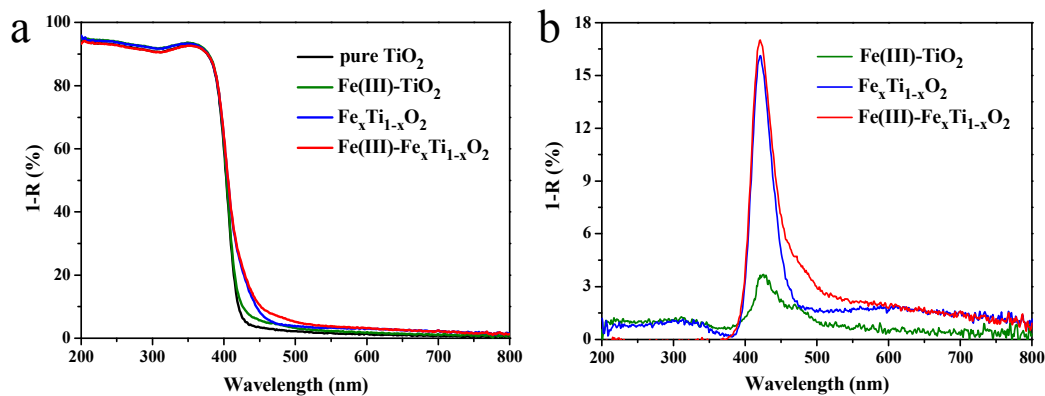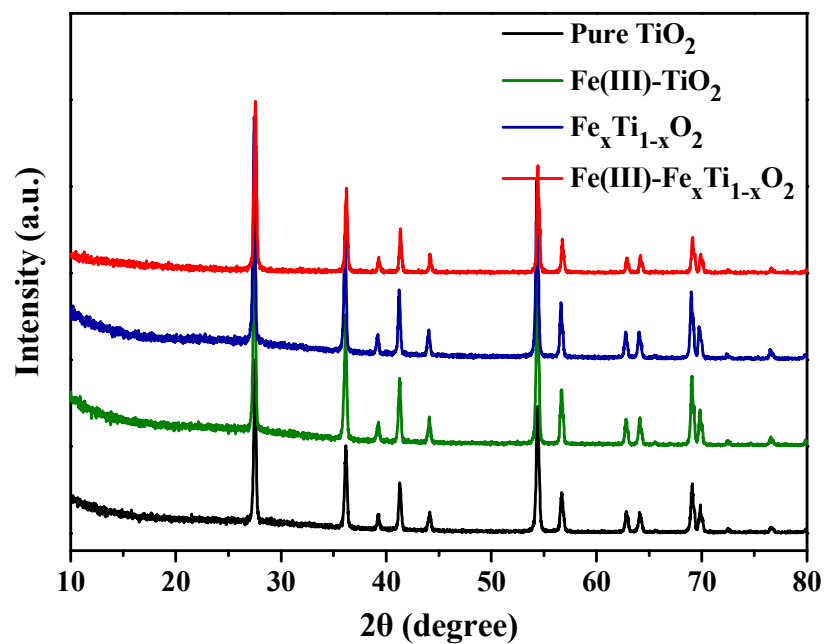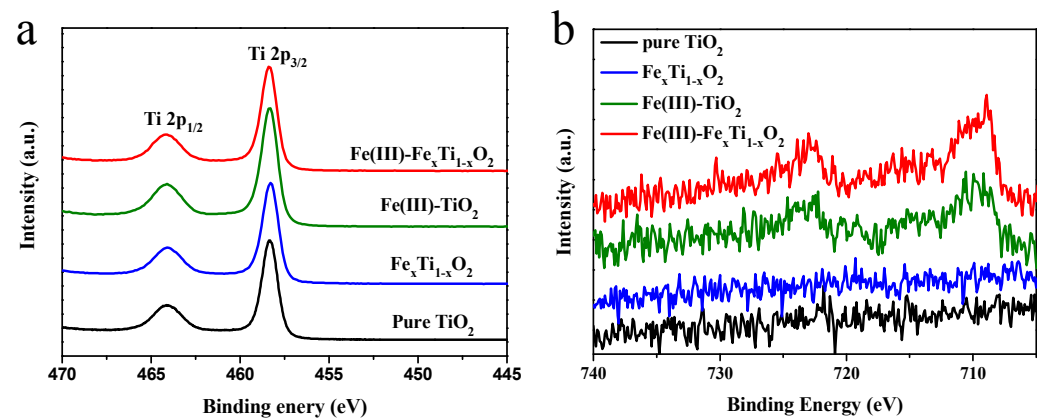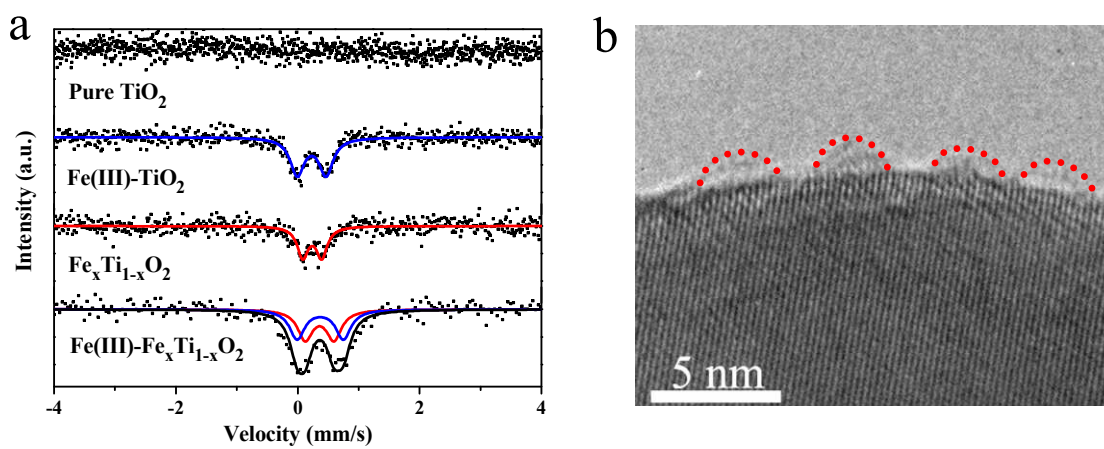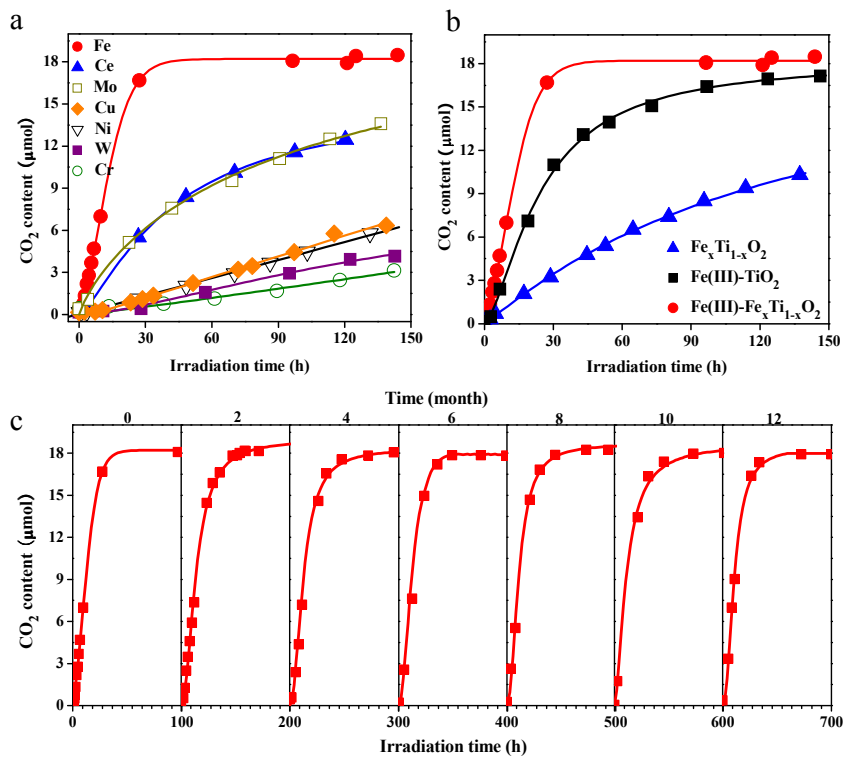
21

Figure 1.

Figure 2.

Figure 3.

Figure 4

Figure 5.

Figure 6.

Figure 7.

Table of contents

Visible light

CB

Fe(III)

Fe(III)

TiO$_2$

VB

h$^+$

multi-electron reduction

oxidation